10. R. L. Hervig, J. V. Smith, J. B. Dawson, *R. Soc. Edinburgh Trans. Earth Sci.* **77**, 181 (1986).
11. D. Mosely, *Am. Mineral.* **66**, 976 (1981).
12. M. R. Drury and H. L. M. van Roermund, *Geology* **16**, 1035 (1988); *ibid.* **17**, 676 (1989); R. L. Hervig, *ibid.*, p. 675.
13. H. W. Green II and Y. Gueguen, *Tectonophysics* **92**, 71 (1983); H. W. Green II, in *Point Defects in Minerals*, R. N. Schock, Ed. (American Geophysical Union, Washington, DC, 1985), pp. 226–233.
14. P. E. Champness, *Mineral. Mag.* **37**, 790 (1970).
15. If H_2O were involved in this reaction, as it can be in the dissolution of trivalent cations in β-olivine, the ratio of the two phases could be somewhat different and a fluid phase could be an additional product. However, we found no microstructural evidence of involvement of a fluid phase [T. E. Young, H. W. Green II, A. Hofmeister, D. Walker, *Phys. Chem. Miner.* **19**, 409 (1993); C. Dupas, N. Doukhan, J.-C. Doukhan, H. W. Green II, T. E. Young, *J. Geophys. Res.* **99**, 15821 (1994)].
16. K. Leinenweber, W. Utsumi, Y. Tsuchida, T. Yagi, K. Kurita, *Phys. Chem. Miner.* **18**, 244 (1991).
17. N. I. Christensen, *Geophys. J. R. Astron. Soc.* **76**, 89 (1984).
18. It is not uncommon that a phase transported out of its stability field should invert not to the stable phase directly but through a cascade of metastable phases, each of which has a lower free energy than does the preceding phase [see A. R. Verma and P. Krishna, *Polymorphism and Polytropism in Crystals* (Wiley, New York, 1966)]. This progression is called the Ostwald Step Rule [W. Ostwald, *Z. Phys. Chem. (Frankfurt)* **22**, 289 (1897)].
19. S. Wang and H. W. Green II, unpublished data.
20. T. Kawamoto, K. Leinenweber, R. L. Hervig, J. R. Holloway, in *Volatiles in the Earth and Solar System*, K. A. Farley, Ed. (AIP Press, New York, 1995).
21. The abundance of pyroxenes in the rock would appear to rule out titanoclinohumite as a precursor that then decomposed to ilmenite plus olivine. Microstructural evidence also does not favor this interpretation, because symplectic decomposition of titanoclinohumite produces a hydrous fluid phase (for which there is no evidence) and much more $FeTiO_3$ than was observed (unless it also produces substantial MgF_2, for which there also is no evidence). Moreover, symplectic decomposition produces complex three-dimensional intergrowths of the product phases rather than the tightly restricted size distribution, isolation, and shape homogeneity of ilmenite that is observed in Alpe Arami olivine [for examples of this decomposition reaction, see V. Trommsdorff and B. W. Evans, *Contrib. Mineral. Petrol.* **79**, 229 (1980)].
22. F. von Blanckenberg and J. H. Davies, *Tectonics* **14**, 120 (1995).
23. M. Akaogi, E. Ito, A. Navrotsky, *J. Geophys. Res.* **94**, 15671 (1989).
24. J. M. Brown and T. J. Shankland, *Geophys. J. R. Astron. Soc.* **66**, 579 (1981).
25. E. Ito and E. Takahashi, *J. Geophys. Res.* **94**, 10637 (1989).
26. A. Mehta, K. Leinenweber, A. Navrotsky, M. Akaogi, *Phys. Chem. Miner.* **21**, 207 (1994).

27. We thank K. Leinenweber for drawing our attention to the spontaneous inversion of $FeTiO_3$ perovskite to the lithium niobate structure upon decompression; M. Akaogi for helpful correspondence; P. Buseck, J. Holloway, and K. Leinenweber for discussions; and four anonymous reviewers for helpful comments. Supported in part by NSF grants EAR92-19369 and EAR 92-19366.

31 October 1995; accepted 11 January 1996

Constraints on Rates of Granitic Magma Transport from Epidote Dissolution Kinetics

Alan D. Brandon,* Robert A. Creaser, Thomas Chacko

Epidote is stable only at high pressure in granitic magmas but is found in magmas crystallized at shallow crustal levels. This observation suggests qualitatively that magma transport is sufficiently rapid to prevent complete epidote resorption. Experimental measurements of epidote dissolution showed that the presence of epidote implies that magma transport from the deep crust in these systems was rapid and that the transport was by dikes rather than diapirs.

Two different models describe the transport of granitic magma from lower crustal source regions to upper crustal emplacement sites. One model envisions magma transport occurring by diapirism (*1*, *2*). Numerical modeling of diapirism indicates that magma transport rates are slow, ~0.3 m year^{-1} up to at most ≤50 m year^{-1}, and ascent times are 10^4 to 10^5 years (*2*, *3*). An alternate model favors transport by fracture propagation and dike networks; calculated magma transport rates for this process are up to 10^5 times those for diapirism (*4*). This correlation between the rates and mechanisms of granitic magma transport can be used to deduce the magma transport mechanism, provided that an independent estimate of transport rate is available.

Measurements of the rates of granitic magma transport are limited. Ascent rates derived for the 1980 to 1986 eruptions of Mount St. Helens dacite from depths of 8 km range from 1.4×10^5 to 2.2×10^7 m year^{-1} (*5*). Because shallow ascent is driven in part by magma vesicularity, it remains an open question whether such rates also apply to the movement of granitic magmas through the middle and lower crust.

To address this issue, we determined the dissolution rate of epidote in granitic magmas experimentally. We chose epidote for study because it has a magmatic origin in some granitic rocks (*6*) and its stability in granitic magmas is restricted to pressures of ≥600 MPa (depth of 21 km) (*7*). Thus, if the dissolution rate of epidote in granitic magmas at pressures of <600 MPa is known, the presence of epidote in granites crystallized in the upper crust (200 to 300 MPa) can be used to constrain magma ascent rates from the lower crust.

In our experiments, we reacted gem quality epidote with natural granodioritic glass at pressures both above and below the stability limit of magmatic epidote (*8*). A high-pressure experiment (1150 MPa, 780°C, 48 hours) showed no evidence of epidote reaction with the granitic melt (Fig. 1B). We interpret this result to indicate that epidote used in our experiments is stable in granitic melt at high pressure. A time series set of experiments conducted at 750°C and 450 MPa resulted in epidote with irregular crystal boundaries surrounded by a complex reaction rim consisting mostly of quenched melt, with minor amounts of magnetite and plagioclase (Fig. 1A). Rim widths ranged from 3 to 8 μm; rim widths increased in longer experiments (*8*).

The time series data conformed to a parabolic rate law [$x = (D_{\text{app}}t)^{1/2}$], where x is the rim width, D_{app} is the apparent diffusion coefficient, and t is time (*9*) (Fig. 2). This relation implies that rim growth was limited by the diffusion of elements between granitic melt and epidote through the melt reaction rim. For epidote dissolution, Si, Al, Ca, and Fe are important diffusing elements, and their diffusivities in granitic melts are broadly similar (*10*). Using measured rim widths from our experiments (Fig. 2), we calculated a D_{app} of 5×10^{-17} $\text{m}^2\ \text{s}^{-1}$ at 750°C, which is similar to a value of 7×10^{-16} $\text{m}^2\ \text{s}^{-1}$ determined at 757°C in water-saturated aluminosilicate melt (*9*). Our results are also consistent with maximum and minimum diffusion coefficients of 1×10^{-16} and 5×10^{-17} $\text{m}^2\ \text{s}^{-1}$, respectively, derived from near-solidus experiments on epidote-bearing tonalite (*11*). Although elemental diffusivity in granitic melts varies as a function of water content, these effects are limited for the water contents expected in natural epidote-bearing magmas (*12*).

Using these data, we modeled epidote dissolution in granitic magmas as a function of time, crystal size, and temperature. At 750°C, dissolution of 0.7-mm-wide epidote crystals surrounded by granite melt, for example, is complete in <90 years; the dissolution of smaller crystals is considerably faster (Fig. 3). We extrapolated these elemental diffusivities to slightly higher and lower temperatures using measured activation energies for hydrous silicate melts (*10*). At temperatures appropriate for granitic magmas [700° to 800°C (*13*, *14*)], epidote

---

A. D. Brandon, Department of Terrestrial Magnetism, Carnegie Institution of Washington, 5241 Broad Branch Road NW, Washington, DC 20015, USA.
R. A. Creaser and T. Chacko, Department of Earth and Atmospheric Sciences, University of Alberta, 126 Earth Sciences Building, Edmonton, Alberta T6G 2E3, Canada.

*To whom correspondence should be addressed.

crystals of typical widths (0.2 to 0.7 mm) surrounded by granite melt will dissolve in 3 to 200 years. Clearly, if magma transport from the lower crust is slow ($\geq 10^3$ years), epidote will dissolve and evidence of a high-pressure history will be removed. Rapid magma transport ($\ll 10^3$ years) is evidently required for epidote preservation in granitic rocks emplaced in the upper crust. This conclusion is not strongly dependent on the magnitude of elemental diffusivities; even diffusion coefficients one-tenth of those we obtained result in dissolution times for typical epidote crystals of $<10^3$ years.

We applied our model for epidote dissolution to epidote-bearing granitic rocks from the Front Range of Colorado and the White Creek Batholith of British Columbia. Rhyodacite dikes from the Front Range contain phenocrysts of epidote, garnet, aluminous amphibole, biotite, plagioclase, and sanidine in a groundmass of quartz and feldspar, and thermobarometric analysis of these minerals indicates equilibration at 700 to 1200 MPa and 800° to 880°C (*15*). Final crystallization occurred after emplacement at pressures of <200 MPa to produce the fine-grained groundmass assemblage that forms 60 to 75% of the dike (*15*). Epidote from these dikes shows highly corroded margins indicative of dissolution and reaction with magma before dike solidification (Fig. 1C). The dissolution zones are up to 50 μm wide but more typically 10 to 20 μm wide.

Minimum magma transport rates can be calculated from the observation that 0.5-mm-wide epidote crystals are still preserved in the dikes. At 800°C, crystals of this width dissolve in <50 years (Fig. 3). Preservation of 0.5-mm crystals therefore requires a transport rate from a pressure of 600 to 200 MPa of greater than 700 m year^{-1} (*15*). Maximum transport rates are estimated from the observed dissolution zone width of epidote (Fig. 1C), on the assumption that no dissolution occurred beyond that now seen. At 800°C, a 50-μm epidote dissolution zone will develop in <1 year, indicating a maximum ascent rate of 1.4×10^4 m year^{-1}. These transport rates for dikes overlap a theoretical transport rate based on numerical modeling (*4*) and are close to measured ascent rates for upper crustal magma (*5*). This result suggests that there is no large disparity in deep-crustal versus upper-crustal transport rates and, by implication, transport mechanisms.

Magmatic epidote is also widespread in mid-Cretaceous plutons of the Omineca Crystalline Belt of southeastern British Columbia (*16, 17*). One of these plutons, the White Creek Batholith, is zoned with marginal quartz monzodiorite and granodiorite grading to granite at the center (*17, 18*); epidote is widespread in the zone of marginal rocks (1 to 3 km wide) (*17*) and has textural and compositional characteristics typical of magmatic epidote reported elsewhere (*19*). Estimates of final crystallization depth made from the contact aureole mineralogy are 230 to 380 MPa [depth of 8 to 13 km (*16*)]. Similarly, results from the Al-hornblende geobarometer (*20*) yield 210 to 400 MPa (7 to 14 km) derived from analysis of hornblende crystal rims (Table 1).

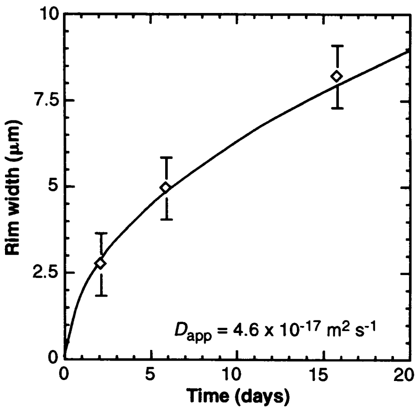

Fig. 2. Time series set of experiments (*8*) at 750°C showing a progressive increase in the reaction rim width with time. The data show a good fit to a parabolic curve, indicating that the reaction rim growth is rate-limited by elemental diffusion in the reaction zone.

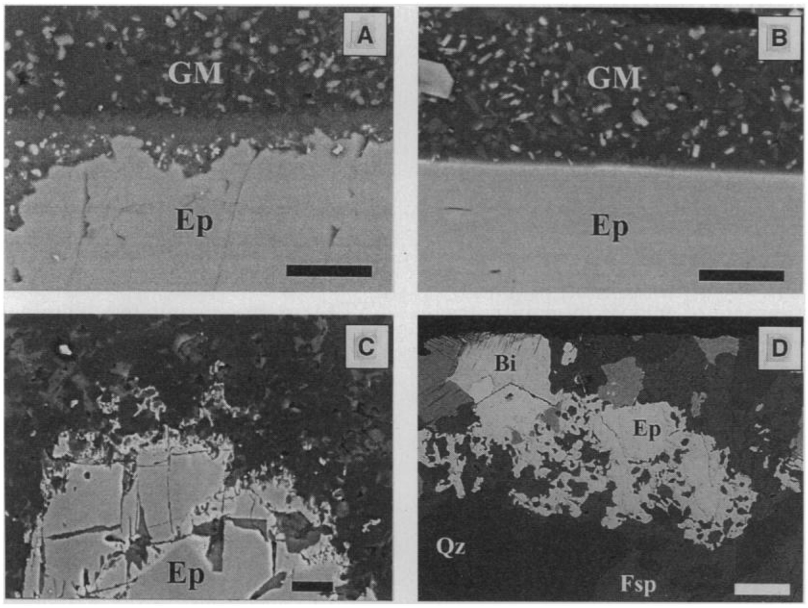

Fig. 1. Backscattered electron images of experimental and natural epidote textures. (**A**) Experimental dissolution of epidote at 450 MPa, 750°C, 379 hours. The reaction zone adjacent to corroded epidote crystal margin separates unreacted epidote (Ep) from granitic melt (GM). The reaction zone contains magnetite, plagioclase, epidote fragments, and granite melt. Scale bar, 10 μm. (**B**) High-pressure experiment (1150 MPa, 780°C, 48 hours) showing no reaction between epidote and granitic melt, demonstrating the high-pressure stability of epidote used in all experiments. Scale bar, 10 μm. (**C**) Epidote from the Colorado Front Range dike (*15*) showing a diffuse, irregular crystal margin indicative of reaction and dissolution with magma. The width of the coherent reacted zone is typically 10 μm, but traces of reacted epidote persist up to 50 μm into the groundmass. Scale bar, 10 μm. (**D**) Epidote from White Creek Batholith sample WC-17 (*17*), southeast British Columbia, showing extensive dissolution in contact with quartz (Qz) and feldspar (Fsp), and unreacted crystal face against biotite (Bi), where epidote was armored from reaction with melt. The small grains in the reacted epidote margin are plagioclase. These reaction textures are common in epidote-bearing rocks from the White Creek Batholith. Scale bar, 100 μm.

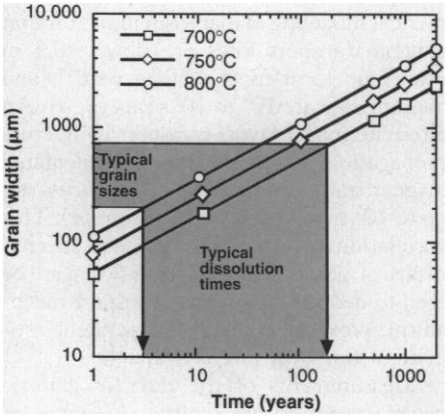

Fig. 3. Dissolution times of epidote crystals in granitic magmas as a function of grain width and temperature. Data at 750°C were calculated from experiments of this study; we calculated the data at 800° and 700°C by extrapolation of the 750°C data using an Arrhenius relation and a typical activation energy of 131 kJ mol^{-1} determined for elemental cation diffusion in hydrous granite melts (*10*). For typical epidote grain widths of 200 to 700 μm, calculated dissolution times range from 2 to 200 years.

Epidote from the White Creek Batholith typically shows perfect crystal faces if enclosed by biotite but is extensively reacted where the same crystal is in contact with quartz or feldspar (Fig. 1D). This texture indicates that epidote is preserved by armoring when isolated from melt contact but also that this epidote was partially exposed to melt, now represented by quartz and feldspar. We interpret such textures to result from epidote-melt reaction during magma ascent and low-pressure crystallization. At least 200 μm has been dissolved from epidote crystals in the White Creek Batholith, which at 800°C would require <13 years for dissolution provided that epidote was in direct contact with melt. In turn, this corresponds to an average ascent rate from 600 MPa to the time of final crystallization of ≥700 m year^{-1}.

The only possibility for epidote preservation at considerably slower magma transport rates would be complete armoring of epidote in mineral aggregates of biotite, quartz, and feldspar. For the margins of the White Creek Batholith, then, the reacted epidote boundaries with quartz and feldspar would demand extensive crystallization of felsic minerals during slow magma ascent. We consider this possibility unlikely because a large proportion of the felsic minerals crystallized at near-solidus temperatures. For example, a haplogranitic melt with a moderate initial water content (3.5% by weight) will remain more than 75% molten to within 40°C of the solidus (*21*). Many high-level granitic magmas (including White Creek) must have been emplaced at temperatures more than 100°C above their solidus, as indicated by the occurrence of up to migmatite-grade contact aureoles. Therefore, upon emplacement, these magmas likely contained only a small proportion of crystallized felsic minerals [<10% (*21*)]. Armoring by felsic minerals is much more likely to occur near the solidus (that is, at the emplacement site) rather than during magma ascent.

The observations from the margin of the White Creek Batholith, like those from the Front Range dikes, suggest that granitic magma was transported rapidly from the lower crust to the upper crust. The magma transport rates we deduced are consistent with rates calculated for fracture propagation in dikes (*4*) but are at least two orders of magnitude faster than the most rapid magma transport rate calculated for diapiric magma ascent at midcrustal levels. A dike transport mechanism is self-evident for the Front Range dikes, but direct evidence for dike transport is lacking for the margins of the White Creek Batholith at current levels of exposure. On the basis of preserved magmatic epidote, we propose that at least the outer zone of the White Creek Batholith is a low-pressure inflation product of dike-transported magma [see also (*4*)].

Preservation of epidote at low pressure also constrains time scales of crystallization processes in upper crustal granitic magma chambers. For the margins of the White Creek Batholith, epidote must have been rapidly removed from melt contact during low-pressure crystallization. Epidote is found only in the marginal quartz monzodioritic and granodioritic rocks, which show geochemical and textural evidence for an origin as crystal cumulates (*17*). We suggest that rapid formation of these cumulates and concomitant expulsion of melt is a viable method of epidote preservation at low pressure. This process must have been more rapid than typical time scales for epidote dissolution (<10^2 years).

Table 1. Chemical analyses (percentages by weight) of experimental and natural materials used (*8*). Columns labeled 1 and 2 show the starting materials, and columns labeled 3 and 4 show the products used for epidote dissolution experiments; granodiorite is WC-21 (*17*). Columns labeled 5 and 6 give representative chemical analyses of hornblende and epidote from White Creek Batholith sample WC-19 (*17*). Analyses were by wavelength-dispersive x-ray microanalysis at the University of Alberta on an ARL-SEMQ electron microprobe (except 2), with an accelerating potential of 15 kV and a current of 12 nA; standards were natural silicates. In the data reduction we used the Phi-Rho-z program (Noran Instruments). Ps, pistacite content [see (*19*)]; NA, analysis not done.

Oxide	1 Epidote (*n* = 8)	2 Granodiorite (volatile-free)	3 Melt (*n* = 5)	4 Melt (volatile-free)	5 Hornblende WC-19 (*20*)	6 Epidote WC-19
SiO_2	37.10	66.90	72.67	78.55	46.69	37.47
TiO_2	0.07	0.63	0.13	0.14	0.91	0.02
Al_2O_3	20.76	15.12	12.23	13.22	7.88	23.25
FeO		3.74	0.76	0.83	15.03	
Fe_2O_3	16.44					13.71
MnO	0.29	0.07	0.03	0.03	0.55	0.18
MgO	0.06	1.90	0.17	0.18	11.07	0.13
CaO	22.56	3.49	1.21	1.31	12.76	22.44
Na_2O	NA	3.36	1.55	1.68	1.10	NA
K_2O	NA	4.32	3.76	4.06	0.73	NA
Total	97.28	100.00	92.51	100.00	98.71	97.23
Ps	34					27
Ps range (*n* = 4)						26–29

The presence of magmatic epidote in granites is not, by itself, sufficient to establish high-pressure granite solidification or to invoke low-pressure stability limits for magmatic epidote beyond those indicated experimentally (*22*). Epidote with reaction textures similar to samples from the White Creek Batholith has been described [figures 2A and 2B of (*6*)] from localities where the Al-hornblende geobarometer (*20*) indicates pressures below or overlapping the epidote low-pressure stability limit [530 to 600 MPa (PJR geobarometer) and 680 to 725 MPa (PS geobarometer); see (*20*)]. In such cases, the significance of epidote as an indicator of initial crystallization of deep crustal magma and as a potential monitor of magma ascent rates to the upper crust should be recognized.

REFERENCES AND NOTES

1. H. Ramberg, *J. Geophys. Res.* **77**, 877 (1972); C. F. Miller, E. B. Watson, T. M. Harrison, *Trans. R. Soc. Edinburgh* **79**, 135 (1988).
2. K. I. Mahon, T. M. Harrison, D. A. Drew, *J. Geophys. Res.* **93**, 1174 (1988).
3. R. F. Weinberg and Y. Podladchikov, *ibid.* **99**, 9543 (1994).
4. J. D. Clemens and C. K. Mawer, *Tectonophysics* **204**, 339 (1992); N. Petford, R. C. Kerr, J. R. Lister, *Geology* **21**, 845 (1993); N. Petford, *J. Geophys. Res.* **100**, 15735 (1995).
5. R. Scandone and S. D. Malone, *J. Volcanol. Geotherm. Res.* **23**, 239 (1985); W. W. Chadwick, R. J. Archuleta, D. A. Swanson, *J. Geophys. Res.* **93**, 4351 (1988); M. J. Rutherford and P. M. Hill, *ibid.* **98**, 19667 (1993).
6. E-an Zen and J. M. Hammarstrom, *Geology* **12**, 515 (1984).
7. M. T. Naney [*Am. J. Sci.* **283**, 993 (1983)] synthesized epidote in granodiorite melts at 800 MPa but not at 200 MPa, and the derived epidote stability curve intersects the granite melting curve at 600 MPa (*6*). M. W. Schmidt [*Contrib. Mineral. Petrol.* **110**, 304 (1992)] experimentally produced epidote only at >750 MPa in granodiorite and at >600 MPa in tonalite. Schmidt (*11*) experimentally produced epidote only at ≥600 MPa in near-solidus experiments with natural tonalite. Schmidt and A. B. Thompson (*Am. Mineral.*, in press) show that the hypersolidus stability field of epidote can be extended to 400 MPa, but only at exceptionally oxidizing conditions (hematite-magnetite buffer) close to the solidus (680°C).
8. Starting materials (Table 1) were (i) crystal-free granitic glass made by melting epidote-bearing granodiorite powder at 950°C and 900 MPa under water-saturated conditions, and (ii) gem-quality epidote with a composition similar to that of most magmatic epidote. Each experimental charge consisted of a 1- to 1.5-mm^3 fragment of epidote, tightly packed with finely ground granite glass sealed into a gold capsule. We performed experiments in a piston cylinder apparatus, using 1.905-cm (outside diameter) NaCl pressure cells of modified Kushiro design [I. Kushiro, *J. Geophys. Res.* **81**, 6347 (1976)]. No corrections were applied to pressures as measured with a Heise bourbon tube gauge. Temperature was measured with W-WRe thermocouples situated directly above the capsule. Temperatures and pressures are believed accurate to ±10°C and ±50 MPa, respective-

ly. The oxygen fugacity (fO_2) of the experiments was not buffered externally. However, fO_2 calculations based on biotite-sanidine-magnetite-H_2O-O_2 equilibrium [D. R. Wones, *Kozan Chishitsu* **31**, 191 (1981)] yield fO_2 values 1.5 to 2 log units above the nickel–nickel oxide buffer. This is consistent with the estimated fO_2 conditions of natural epidote-bearing magmas (*6, 16*). Quenched experimental charges were sectioned longitudinally, polished, and examined with reflected-light microscopy and backscattered electron imaging. Rim widths were measured with an optical microscope equipped with a graduated ocular lens; the rim widths reported are the average of 20 to 30 measurements. Rim width data are as follows: experiment Ep-10, t = 51.17 hours, rim width = 2.74 ± 0.9 μm; experiment Ep-12, t = 141.20 hours, rim width = 4.95 ± 0.8 μm; and experiment Ep-11, t = 378.78 hours, rim width = 8.18 ± 1.3 μm.

9. D. C. Rubie and A. J. Brearley, in *High-Temperature Metamorphism and Crustal Anatexis*, J. R. Ashworth and M. Brown, Eds. (Unwin Hyman, London, 1988), pp. 57–86. See also G. W. Fisher, *Geochim. Cosmochim. Acta* **42**, 1035 (1978).
10. D. R. Baker, *Contrib. Mineral. Petrol.* **106**, 462 (1991).
11. M. W. Schmidt [*Am. J. Sci.* **293**, 1011 (1993)] conducted four experiments on epidote-bearing tonalite from which minimum and maximum apparent diffusion coefficients can be estimated. Three experiments (r29 through r31) below the epidote low-pressure stability limit (≤450 MPa) showed no trace of epidote (maximum size, 10 μm) after 500 to 504 hours at temperatures of 680° to 700°C in addition to an initial period of ≥30 hours at 720° to 750°C. These data yield a minimum D_{app} of 5×10^{-17} m^2 s^{-1}. One experiment (r28) yielded an epidote rim of ≤4 μm at 600 MPa and 720°C for ≥30 hours, from which a maximum D_{app} of 1×10^{-16} m^2 s^{-1} can be estimated.
12. Diffusivity of cations in granitic melts varies as a function of melt structure, viscosity, and water content, all of which are interrelated (*10*). Water contents of our experiments (estimated at 7.5% H_2O from totals, Table 1) agree well with expected 450-MPa water saturation conditions [C. W. Burnham, in *Geochemistry of Hydrothermal Ore Deposits*, H. L. Barnes, Ed. (Holt, Rinehart and Winston, New York, 1967), pp. 34–76] and will yield the highest diffusivities at this pressure. For lower magma water contents, magma viscosity will be higher and diffusivities will be lower, yielding longer estimates of dissolution time. However, changes in magma viscosity as a function of water content are most striking from 0 to 2% H_2O and small above 4% H_2O, and the effects of viscosity on diffusivity at high water contents should be relatively small. Differences in diffusivity of just one order of magnitude have been documented between granitic melts with 3% H_2O and 6% H_2O (*10*), which spans the range of natural granitic melt water contents [J. D. Clemens, *Lithos* **17**, 273 (1984)], and diffusivity differences of this magnitude have little significance for the conclusions drawn here.
13. Temperatures up to 850°C are typical for granitic magmas [(*16*); J. A. Whitney and J. C. Stormer, *J. Petrol.* **26**, 726 (1985)]. For extrapolation of the 750°C D_{app} values to other temperatures, an activation energy of 131 kJ mol^{-1} was used (*10*).
14. W. Johannes, *Contrib. Mineral. Petrol.* **86**, 264 (1984).
15. B. W. Evans and J. A. Vance, *ibid.* **96**, 178 (1987); R. L. Dawes and B. W. Evans, *Geol. Soc. Am. Bull.* **103**, 1017 (1991).
16. D. A. Archibald, T. E. Krogh, R. L. Armstrong, E. Farrar, *Can. J. Earth Sci.* **21**, 567 (1984); A. D. Brandon and R. St.J. Lambert, *ibid.* **30**, 1076 (1993).
17. A. D. Brandon and R. St.J. Lambert, *J. Petrol.* **35**, 239 (1994). Only the outer margin of the batholith (zone 1 to 3 km thick) has abundant epidote (from 0.1 to 3%). The middle-zone granodiorite has only minor or no epidote (less than 0.1%). The two-mica granite, for which there is geochemical evidence that it is derived from a different crustal source, has no epidote. The latter two zones are >60% of the areal exposure. Epidote in these inner zones was either completely resorbed or was never stable in these more felsic magmas.
18. J. E. Reesor, *Geol. Surv. Can. Mem. 292* (1958).
19. Epidote from the White Creek Batholith shows textures indicative of magmatic origin. These include euhedral crystal forms where protected from reaction by biotite, and cores of allanite [see (*6, 16*)]. Magmatic epidote in granites typically has <0.2% TiO_2 by weight (*6, 16, 22*), whereas secondary epidote replacing biotite has >0.6% TiO_2 (*15*). Epidote from the White Creek Batholith has <0.1% TiO_2 (Table 1). The pistacite (Ps) content of magmatic epidote (Ps = molar $[Fe^{3+} / (Fe^{3+} + Al)] \times 100$) ranges from Ps_{23} to Ps_{29} [(*6*); M. T. Naney, see (*7*)]. Secondary epidote replacing plagioclase has a lower Ps content (Ps_{0-24}), and secondary epidote replacing biotite has a higher Ps content (Ps_{36-48}) [A. J. Tulloch, *Contrib. Mineral. Petrol.* **69**, 105 (1979)]. Epidote from the White Creek Batholith (Ps_{26-29}) overlaps the magmatic range (Table 1).
20. Epidote-bearing granodiorites from the White Creek Batholith have mineral assemblages appropriate for use of the Al-hornblende geobarometer [J. M. Hammarstrom and E-an Zen, *Am. Mineral.* **71**, 1297 (1986)] based on recent experimental calibrations [M. C. Johnson and M. J. Rutherford, *Geology* **17**, 837 (1989) = PJR below; M. W. Schmidt (*7*) = PS below]. See Table 1 for a typical hornblende analysis. For this analysis, we obtained pressures of 240 and 360 MPa, respectively, using the PJR and PS geobarometers. For 16 hornblende analyses from samples WC-18 and WC-19, we obtained a range of 210 to 280 MPa and a mean of 240 MPa (depth of 8.4 km) using the PJR geobarometer, and a range of 320 to 400 MPa and a mean of 360 MPa (depth of 12.6 km) using the PS geobarometer.
21. H. Nekvasil, *Am. Mineral.* **73**, 966 (1988).
22. C. R. Vyhnal, H. Y. McSween, J. A. Speer, *ibid.* **76**, 176 (1991); A. J. Tulloch, *Geology* **14**, 186 (1986); R. H. Moench, *ibid.*, p. 187.
23. We thank B. Evans and R. Dawes for sample material, R. W. Luth for laboratory facilities, M. Walter for initial experiments, A. Locock for the epidote sample, P. Wagner for electron microprobe assistance, and P. Resultay for timely polishing of the charges, and R. W. Luth, J. Farquhar, D. R. M. Pattison, and three anonymous reviewers for helpful comments. Supported by Natural Sciences and Engineering Research Council of Canada research grants to R.A.C. and T.C. A.D.B. is supported by a Carnegie Institution Post-Doctoral Fellowship.

20 September 1995; accepted 16 January 1996

Enhancement of Solution NMR and MRI with Laser-Polarized Xenon

G. Navon,* Y.-Q. Song, T. Rõõm, S. Appelt, R. E. Taylor, A. Pines†

Optical pumping with laser light can be used to polarize the nuclear spins of gaseous xenon-129. When hyperpolarized xenon-129 is dissolved in liquids, a time-dependent departure of the proton spin polarization from its thermal equilibrium is observed. The variation of the magnetization is an unexpected manifestation of the nuclear Overhauser effect, a consequence of cross-relaxation between the spins of solution protons and dissolved xenon-129. Time-resolved magnetic resonance images of both nuclei in solution show that the proton magnetization is selectively perturbed in regions containing spin-polarized xenon-129. This effect could find use in nuclear magnetic resonance spectroscopy of surfaces and proteins and in magnetic resonance imaging.

Sensitivity poses a persistent challenge to nuclear magnetic resonance (NMR) spectroscopy and magnetic resonance imaging (MRI). One problem is low spin polarization, the very small population difference between "up" and "down" spins, which is usually no more than 1 in 10^5 at thermal equilibrium at room temperature. Lower temperatures and higher fields can provide only limited relief, so spectroscopists have resorted, instead, to schemes such as optical pumping and dynamic nuclear polarization in order to enhance the polarization.

Optical pumping (OP) methods (*1*) transfer angular momentum from circularly polarized light to electronic and nuclear spins. The exchange of angular momentum, often accomplished in one or more steps, reorients the spins and thus alters the polarization. After OP effects were shown for the nuclear spins of gaseous ^3He in a He/Rb mixture (*2*), the method was subsequently further developed at Princeton for ^{129}Xe as well as ^3He (*3*). The strong NMR signals obtained from hyperpolarized gases have since extended the use of high-resolution ^{129}Xe NMR and MRI (*4*), giving rise to a number of experiments, among them enhanced surface NMR of ^{129}Xe (*5*), signal enhancement of proton and ^{13}C NMR by thermal mixing (*6, 7*), and Hartmann-Hahn cross-polarization (*8*), polarized gas gyroscopes (*9, 10*), and, most recently, enhanced MRI of void spaces in organisms (such as the lung) and materials (*11, 12*).

Dynamic nuclear polarization (*13, 14*) arises from the cross-relaxation between coupled spins. When the polarization of one spin species is disturbed, the polarization of a neighboring species deviates from equilib-

---

Materials Sciences Division, Lawrence Berkeley National Laboratory, and Department of Chemistry, University of California, Berkeley, CA 94720, USA.

*Permanent address: School of Chemistry, Tel Aviv University, Tel Aviv 69978, Israel.

†To whom correspondence should be addressed at the Department of Chemistry, University of California, Berkeley, CA 94720, USA.